Research Article

Rice husk: green adsorbent for Pb(II) and Cr(VI) removal from aqueous solution—column study and GA–NN modeling

Tania Mitra[1] · Nirjhar Bar[1] · Sudip Kumar Das[1]

Abstract

Due to the harmful effects of heavy metal ions such as lead, chromium, and others, an economic and eco-friendly removal process using green adsorbent is required to make water bodies safe. Rice husk is used as an adsorbent in continuous column mode for the removal of Pb(II) and Cr(VI) ions. The variations of column process parameters like influent metal concentration, bed height, the rate of flow, etc., are investigated to study the breakthrough behavior. The higher bed height but lower flow rate and influent concentration give the better result. The experimental data fitted well to that of the empirical models. The Thomas model and Yoon–Nelson model fit the experimental data well. GA–ANN-based hybrid network has been used for modeling purpose.

Keywords Rice husk · Fixed-bed adsorption · Thomas model · Yoon–Nelson model · Genetic algorithm

Nomenclature

b	Rate constant for Langmuir isotherm (L mg^{-1})
C_0	Initial metal ion concentration at $t = 0$ (mg L^{-1})
C_t	Output metal ion solution concentration at time t (mg L^{-1})
C_t/C_0	Relative concentration
K_2	Pseudo-second-order rate constant (mg g^{-1} min^{-1})
K_{AB}	Kinetic constant for Bohart–Admas model (L mg^{-1})
k_f	Freundlich constant [(mg g^{-1})/(mg L^{-1})$^{1/n}$]
K_i	Intra-particle rate constant (mg g^{-1} min$^{-1/2}$)
K_{th}	Thomas rate constant (L mg^{-1} min^{-1})
K_{YN}	Yoon–Nelson model constant (min^{-1})
N_0	Saturation concentration (mg L^{-1})
n	Intensity of sorption for Freundlich constants (mg g^{-1})/(mg L^{-1})$^{1/n}$
q_0	Maximum metal uptake capacity (mg g^{-1})
q_{eq}	Equilibrium metal uptake capacity (mg g^{-1})
q_t	Total adsorbed metal ions at time t (mg)
q_{t0}	Total adsorbed metal ions at time $t = 0$ (mg)
q_w	Metal uptake capacity for Wolborska model (g L^{-1} min^{-1})
q_y	Metal uptake capacity for Yoon–Nelson model (mg g^{-1})
R^2	Correlation factor
t	Time of flow (min)
u_0	Linear velocity (m min^{-1})
v	Flow rate (mL min^{-1})
x	Amount of adsorbent present in the column (g)
Z	Bed depth (cm)
β_a	Wolborska rate constant (min^{-1})
τ	50% time for Yoon–Nelson model (min)
AARE	Average absolute relative error AARE $= \frac{1}{N}\sum_{i=1}^{N}\left|\frac{(y_i-x_i)}{x_i}\right|$, dimensionless
MSE	Mean-squared-error, $\frac{1}{N}\sum_{i=1}^{N}(x_i - y_i)^2$, dimensionless

✉ Sudip Kumar Das, drsudipkdas@vsnl.net; skdchemengg@caluniv.ac.in; Tania Mitra, tmchemengg_rs@caluniv.ac.in; Nirjhar Bar, nirjhar@hotmail.com | [1]Department of Chemical Engineering, University of Calcutta, 92, A. P. C. Road, Kolkata, West Bengal 700 009, India.

TF   Transfer function 1 in the hidden layer, $f_{1h}(x) = \tanh \beta x = \frac{e^{\beta x} - e^{-\beta x}}{e^{\beta x} + e^{-\beta x}}$, dimensionless

R^2 Correlation coefficient, $R = \frac{\sum_{i=1}^{N}(x_i - \bar{x})(y_i - \bar{y})}{\sqrt{\sum_{i=1}^{N}(x_i - \bar{x})^2 \sum_{i=1}^{N}(y_i - \bar{y})^2}}$, dimensionless

Greek letters

χ^2 $\chi^2 = \sum_{i=1}^{N} \frac{(x_i - y_i)^2}{y_i}$, dimensionless

σ $\sigma = \sqrt{\sum_{i=1}^{N} \frac{1}{N-1} \left[\left| \frac{(y_i - x_i)}{x_i} \right| - \text{AARE} \right]^2}$, dimensionless

1 Introduction

Nowadays, it becomes a challenge to people worldwide to make the environment safe and pollution free by removing toxic metals like lead, chromium, cadmium, zinc, nickel, copper, etc., from the water stream as these are non-biodegradable. Although some of these heavy metals are necessary for human need in trace amount as micronutrient, the presence of a large amount of these causes serious risk to the human being [30]. Pb(II) and Cr(VI) both are coming to water bodies from the electroplating industries, battery manufacturing industries, paints and pigments, leather tanning industries, ceramic industries, textile and metal finishing, wood preservation, mining industries, etc. [3, 8, 35, 39]. Cr(VI) is very much harmful to the human being as it is carcinogenic and also responsible for skin allergy, stomach problem, problems related to the lung, etc. [8]. Pb(II) is harmful as it causes serious damage to brain, kidney, livers as well as it affects the reproductive system and nervous system [29, 30, 42, 47]. EPA [13], IS [21], and WHO [51] set the discharge limit of these metal ions in the water bodies, and these are 0.1 mg L^{-1} for Pb(II) ion and 0.1 mg L^{-1} according to EPA and IS, 0.05 mg L^{-1} according to WHO for Cr(VI) ion. Chemical precipitation, reverse osmosis, ion exchange, coagulation, adsorption using activated carbon, etc. [12, 19, 48, 49], are used for alleviation of these metal ions. Among them, adsorption using activated carbon is an efficient process, but the high market price of activated carbon and difficulty in regeneration makes limited of its use. The use of activated carbon had been mentioned by many previous researchers in the field of chemistry, but its current market price is high [55]. Hence, our quest is to find out affordable, locally available and environment-friendly adsorbent to treat the wastewater [12, 27, 38].

Rice husk (RH) is a well-known and readily available agricultural waste, in the countries which produce rice in large amount. More than 600 million tonnes of paddy production is recorded in the world, on average 20% of the paddy is husked. The rice husk (RH) production is more than 120 million tonnes/annum [25]. It is also useful to make the bed for animals, as well as it is burned for energy generation or dumped as waste, while the industrial application is still minimal [26, 32].

The main compositions of RH are celluloses (25–35%), hemicelluloses (18–21%), lignin (26–31%), silica (15–17%), soluble (2–5%), and rest moisture [32]. SiO_2, H_2O, Al_2O_3, Fe_2O_3, K_2O, Na_2O, CaO, and MgO are present in the RH as the chemical components [15]. RH contains functional group like carboxyl, hydroxyl, and amidogen, etc., and also contains numerous floristic fiber and protein which make RH as a suitable adsorbent [14, 20, 25, 26, 32].

Most of the third world countries, small- and medium-sized process industries are present in large number which generate Pb(II) and Cr(VI) containing waste stream, but the environment-friendly treatment process is deficient. Hence, the industries immediately require a cost-effective way to treat their waste stream.

In India, a vast number of rural areas are present with small- and medium-scale industries like battery manufacturing industries, wood preservation industries, electroplating industries, etc. These industries provide employment opportunity in rural areas. These industries also generate wastewater containing heavy metals like Pb(II), Cr(VI), Cu(II), etc., which need to be processed before discharge. In rural areas, wastewater treatment facility and common effluent treatment are not available. Hence, for the economic reason, these industries drain their wastewater into the drain line which pollutes the local environment. The present work is to use the available natural agricultural waste like rice husk as adsorbent for heavy metal (Pb(II) and Cr(VI)) separation from wastewater in the continuous model and also discuss the safe disposal of the waste adsorbent. This study is the continuation of the previous work where batch studies were conducted [41, 42]. The variation in different operating parameters, e.g., bed depth, the rate of flow, influent concentration, etc., has been investigated. The column performance predictions have been performed by using different available kinetic models like Thomas, Bohart–Admas, Yoon–Nelson, Wolboska model.

RH is low-cost and widely available material and therefor is tried as an adsorbent in continuous mode operation. The adsorptive capacity is not very high as reported with other adsorbents. Hence, it demands the use higher amount of adsorbents and also bigger sized equipment. This is offset by the advantages of very low cost of the green adsorbent and ease of safe disposal. This green adsorbent is suitable in third world countries for medium- and small-sized industries which generate heavy metals in their wastewater, and where no common treatment facility is available.

Sometimes researchers tried neural network (NN) and genetic algorithm–neural network (GA–NN) modeling for the prediction purpose in various aspects of science/engineering [4–7, 11, 16–18, 34, 43, 44]. The usefulness of GA–ANN hybrid modeling is also investigated.

2 Materials and methods

2.1 Adsorbents preparation

The RH has been collected from a rice mill, at Bandel, Hooghly district, West Bengal. Distilled water was used to wash the RH several times to wash out the dust particles and dried in an oven at 60–65 °C for 8 h. The adsorbent was screened, and the fraction of − 44 + 52 mesh was used to prepare the bed in the column.

2.2 Metal solution preparation

The standard stock solution of 10^3 mg L^{-1} concentrated of Pb(II) and Cr(VI) has been prepared by mixing 1.61 g of $Pb(NO_3)_2$ and 2.83 g of $K_2Cr_2O_7$ in distilled water. Proper dilution had been done to get the desired initial concentration of Pb(II) as well as Cr(VI) ion solution as required using the stock solution. The analytical grade chemicals have been used in this study. These chemicals are purchased from the market (E. Merck India Limited) located in the city of Mumbai, India.

2.3 Instruments used

The pH meter [Multi 340i (WTW)] has been used in this study. It has been previously calibrated with the help of standard buffer solutions. The Peristaltic pump (Cole-Parmer, model-73 7535-04, USA) has been used for the flow of metal ion solution to the column. Atomic absorption spectrophotometer (AA 240 VARIAN, Australia) has been used for the measurement of the Pb(II) ion concentration, and UV–Vis spectrophotometer (Dr 5000, HACH USA) has been used to measure the Cr(VI) ion concentration. Scanning electron microscope (S-3400N; Hitachi, Japan) has been used to observe the texture of the surface RH. The responsible and active functional groups which are present in the adsorbent have been determined using 'Fourier transform infrared spectroscopy' (Alpha FTIR, Bruker, Germany). Micromeritics surface area analyzer (ASAP 2020) is used to measure the BET surface area of RH. The moisture content present in the RH has been determined using moisture analyzer (Mettler LP16). The solid addition method has been used to determine the point of zero charge [41].
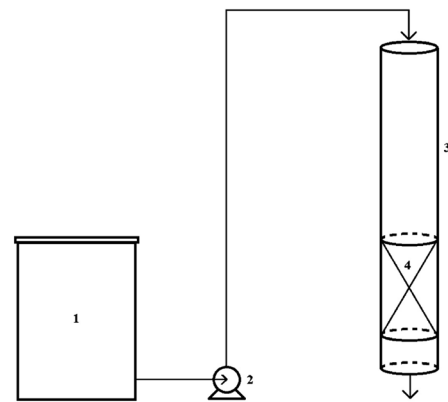
1. Feed storage, 2. Peristaltic pump, 3. Glass column, 4. Adsorbent

Fig. 1 Schematic diagram of the column

Table 1 Physical properties of rice husk [41]

Surface area (m^2/g)	0.54
Bulk density (g/cm^3)	0.54
Point of zero charge (pH)	6.05
Moisture content (%)	9.02
Dry matter content (%)	90.98
Ash content (%)	11.80

3 Experimental

The column performances are operated in three glass columns, each having an inner radius of 0.9 cm along with 50 cm height. The lowest point of the column has been mechanically supported by metal sieve plate, and 0.5 mm of glass wool has been kept over the sieve plate to prevent any loss of the adsorbent. The adsorbent is placed within the glass column to make the bed, and distilled water is added to settle the bed at desired heights. After the settlement of bed height, the water has been drained out from the column. The metal ion solution of the desired initial concentration has been introduced into the column by using a peristaltic pump at the desired flow rate. The necessary samples are collected at the point of exit from the column at different time intervals. The room temperature of 25 ± 2 °C has been maintained during the whole experiments. The diagram of the column is presented schematically in Fig. 1.

3.1 Adsorbent characterization

The physical properties of the RH are shown in Table 1. Figure 2 represents the scanning electron micrograph
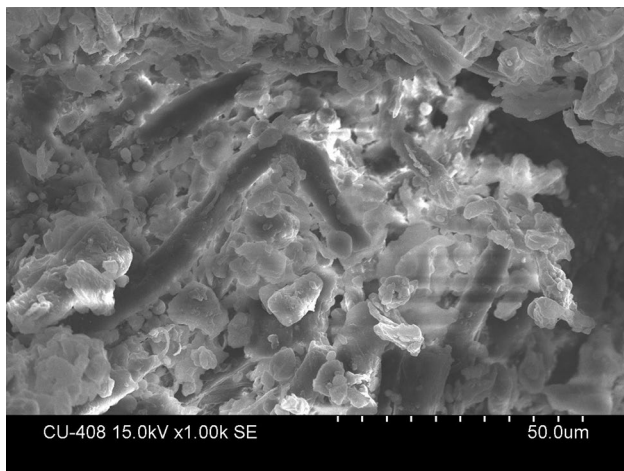
Fig. 2 Scanning electron micrograph of rice husk

(SEM) of RH, and it indicates the porous structure of the adsorbent.

3.1.1 FTIR study

Table 2 represents the shift in wave number range from 4000 to 400 cm^{-1} for fresh and metal-loaded biomass. FTIR study is done to specify the functional groups that are present within the adsorbent that is responsible for Pb(II) ion and Cr(VI) ion adsorption [42]. From the table, the shift in wave number from 3385.42 cm^{-1} (fresh RH) to 3465.04 cm^{-1} (Pb(II) ion adsorbed RH) and 3421.10 cm^{-1} (Cr(VI) ion adsorbed RH) indicates the responsibility of surface –OH group for adsorption. Unsaturated group like alkene is found to be responsible for adsorption as the peak shift from 1654.62 cm^{-1} (fresh RH) to 1634.46 cm^{-1} [Pb(II) ion adsorbed RH] and 1638.23 cm^{-1} [Cr(VI) ion adsorbed RH]. The C–NO$_3$ group is also showed the intense band around 1515.77 cm^{-1} (fresh RH) which shifts to 1532.46 cm^{-1} [Pb(II) ion adsorbed RH] and 1509.99 cm^{-1} [Cr(VI) ion adsorbed RH] for Pb(II) and Cr(VI) ion adsorption.

3.2 Analysis of metal ion solution [2]

The concentration of Pb(II) ion has been measured with the help of the Atomic Absorption Spectrophotometer (AA 240 VARIAN, Australia). The concentration of the Cr(VI) ion has been measured with the help of UV–Vis spectrophotometer (Dr 5000, HACH USA), and a complexing agent (1,5–diphenylcarbazide) has been used for the analysis of the Cr(VI) ion concentration at 540 nm.

4 Results and discussion

The column experiment data are explained from the plot of the relative concentration (ratio of the effluent metal ion concentration to that of the influent metal ion concentration) versus contact time. The total adsorbed metal ion for a specific flow rate is evaluated as,

$$q_t = \frac{v}{1000} \int_{t_0}^{t_s} C_{ad} \mathrm{d}t \tag{1}$$

The equilibrium metal ion uptake depends on the weight of the adsorbent as,

$$q_{eq} = \frac{q_t - q_{t0}}{x} \tag{2}$$

4.1 Effect of initial pH

Our earlier experiment has been conducted from pH 2–6, and experimental investigation has reported that maximum adsorption for Pb(II) ion takes place when the pH level is 5 [42]. At lower pH, the H$^+$ ions and Pb(II) ions compete with each other for the occupation of the free binding sites of the adsorbent. This makes the process complicated and less effective. As the pH of the solution tends to increase, the functional groups start to activate, which increase the adsorption of Pb(II) ion. Moreover, pH more than 5 has resulted in the precipitation of Pb(OH)$_2$

Table 2 Wave number (cm) for the dominant peak from FTIR for Pb(II) and Cr(VI) adsorption

Functional group	Raw rice husk	Pb(II) ion loaded rice husk	Cr(VI) ion loaded rice husk
Surface O–H stretching	3385.42	3465.04	3421.10
Aliphatic C–H stretching	2925.48	2921.41	2925.48
Aldehyde C–H stretching	2854.13	2851.26	2854.13
Unsaturated group like alkene	1654.62	1634.46	1638.23
Aromatic C–NO$_2$ stretching	1515.77	1532.46	1509.99
Si–O stretching	1098.26	1031.58	1075.12

which makes a combined process of adsorption and precipitation. Hence, the whole experiment has been carried out at pH 5.

Similarly, our earlier investigation was carried out from pH 1–6, which shows that maximum sorption of the Cr(VI) ion onto the RH at pH 1.5 [41]. With lower pH, Cr(VI) ion exists in $HCrO_4^-$ form. As pH increases from 2 to 6, Cr(VI) ion exist in the form of $Cr_2O_7^{2-}$, $HCrO_4$, $Cr_3O_{10}^{2-}$, in which $HCrO_4^-$ predominates. At pH higher than 6, the process is not significant due to the formation of a complex of negative ions of CrO_4^{2-}, $Cr_2O_7^{2-}$ and OH^- in which the latter predominates due to its less size among them.

4.2 Effect of bed height

Figures 3 and 4 represent the breakthrough curves for three different bed heights, i.e., 4–10 cm for Pb(II) as well as Cr(VI) ion adsorption, respectively. The capacity of metal uptakes of the adsorbent is higher at the beginning of the process but rapidly decreases after the breakthrough time. The higher bed depth takes more time for saturation than lower bed depth. The breakthrough and exhaustion time both have a tendency to increase with the increased bed height, and this occurs as more amount of adsorbent are present and the presence of free adsorption sites in the bed [22, 28, 34, 45, 50]. With the decrease in bed height from 10 to 4 cm, it results in
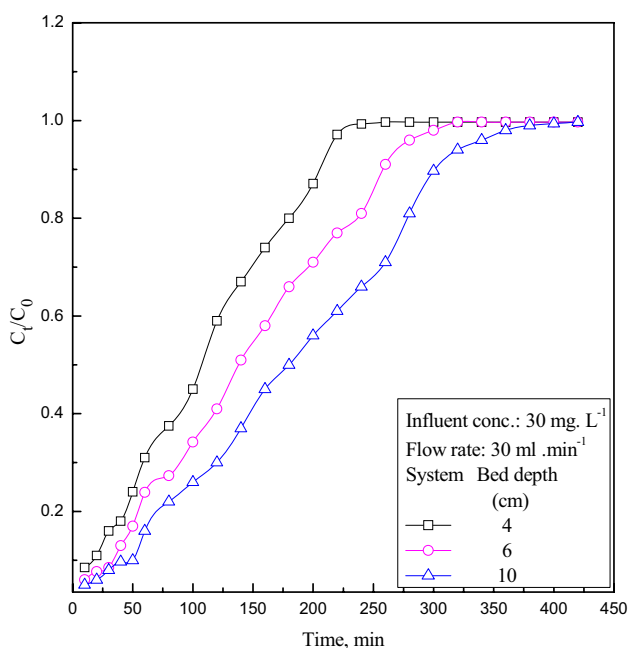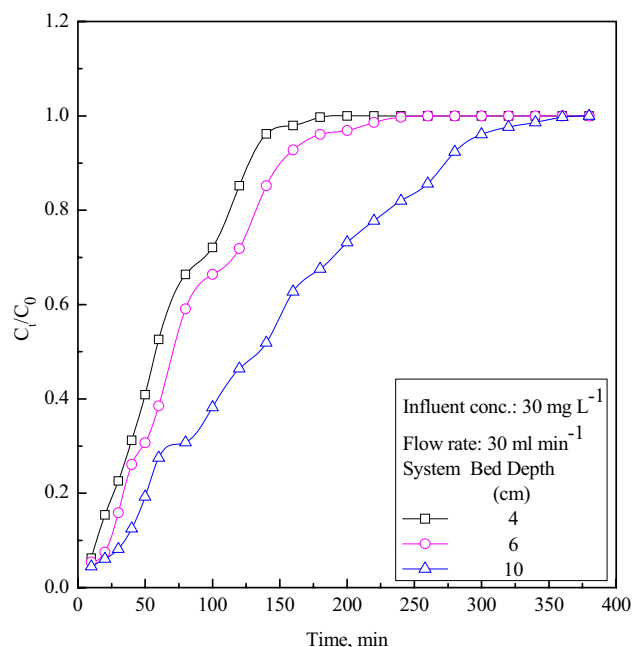

Fig. 4 Effect of bed depth for Cr(VI) ion removal

the steepness of the breakthrough curve which shifts the left side of the time axis.

4.3 Effect of flow rate

The rate of flow is varied from 10 to 40 mL min^{-1} in this study. The impact of the change in rates of flow for the removal of Pb(II) as well as Cr(VI) ions is shown in the Figs. 5 and 6, respectively. It is observed from these figures that there are sharp increases in the breakthrough curves as the rate of flow increases. At high flow rate, the concerned metal ions get less time for the contact with the adsorbent and represent a steep breakthrough curve. The external film mass resistance and residence time both are decreased which result in the less saturation time and less removal efficiency [10, 31, 43]. As the flow rate is increased from 10 to 40 mL min^{-1}, the equilibrium metal uptake has also been increased from 13.86 to 39.16 mg L^{-1} for Pb(II) ions, and no general trend has been observed for Cr(VI).

4.4 Effect of initial concentration

Figures 7 and 8 show the representative graph on the variation in initial concentration of the metal ion on bed height of 4 cm for Pb(II) and Cr(VI) ion, respectively. It is explicit from the figures that the breakthrough and saturation time both are faster at the higher influent concentration [36]. The adsorbents are saturated very fast by covering all free adsorption sites by metal ions at a higher concentration than the lower one [23, 33].

Fig. 3 Effect of bed depth for Pb(II) ion removal

Fig. 5 Effect of flow rate for Pb(II) ion removal
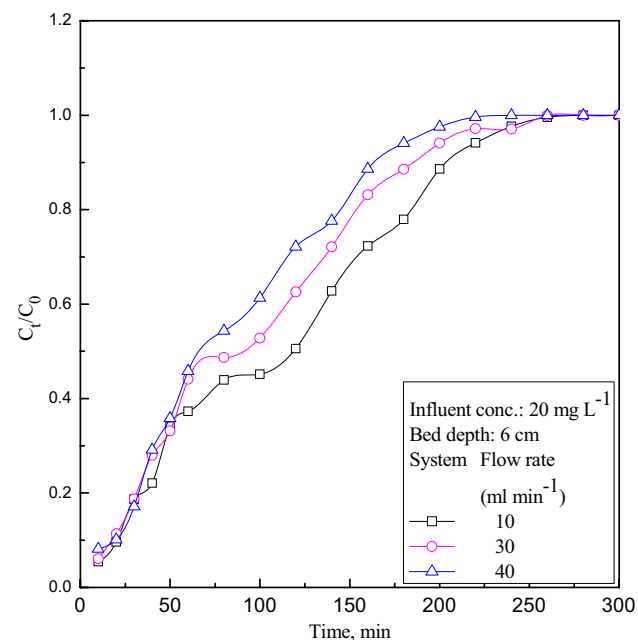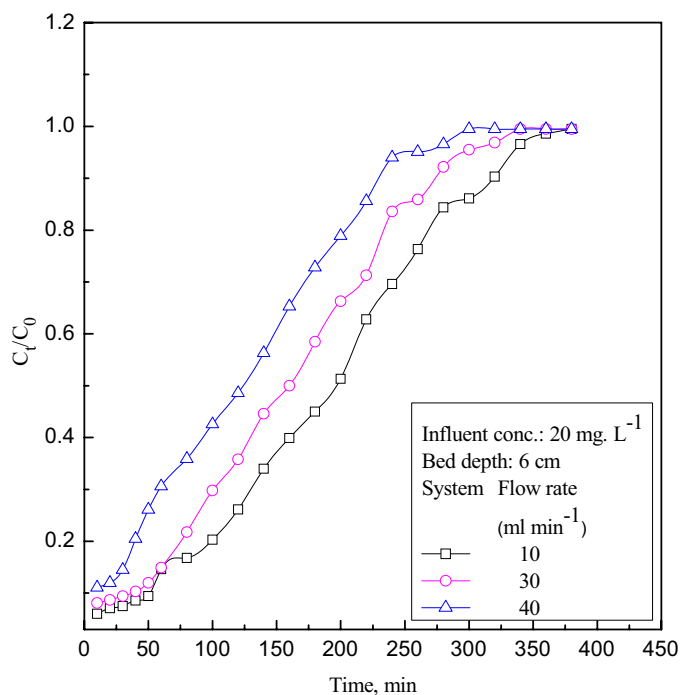
Fig. 6 Effect of flow rate for Cr(VI) ion removal
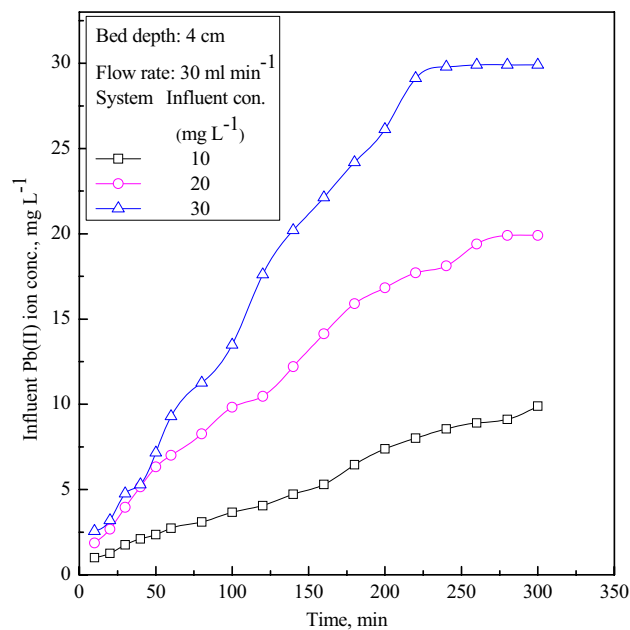
Fig. 7 Effect of influent Pb(II) ion concentration on the removal

Hence, at higher concentration, the adsorption efficiencies are lower than that of the lower metal ion concentration. The increasing influent concentration indicates the increased metal uptake capacity of adsorbent from 5.72 to 22.99 mg L^{-1} for Pb(II) ion and 2.798–10.18 mg L^{-1} for Cr(VI) ion, respectively. Researchers have also shown a similar result [1, 50].

4.5 Isotherm and kinetics

The earlier study [41, 42] has reported the isotherm and kinetic studies in detail. Table 3 represents the model parameters concerning both the ions. Both Langmuir isotherm along with Freundlich isotherm model are in good agreement. The intra-particle diffusion model is well
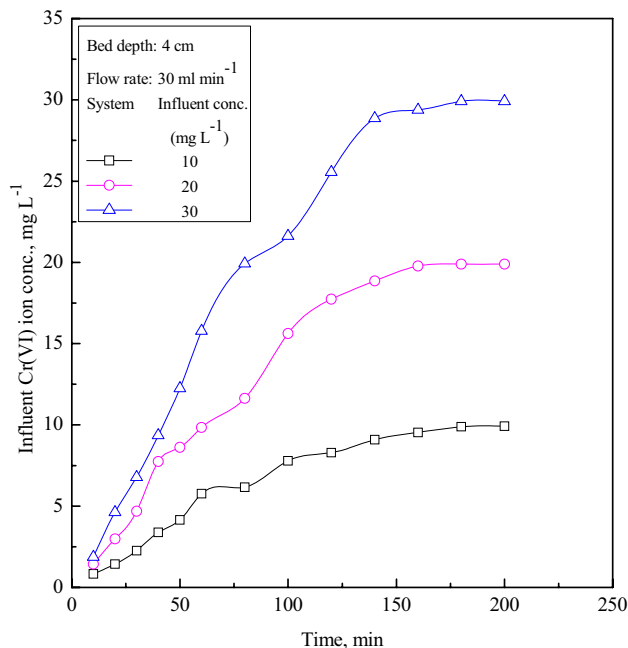
Fig. 8 Effect of influent Cr(VI) ion concentration on the removal

described for Pb(II) removal, and pseudo-second-order model has been applied well for Cr(VI) removal.

4.6 Modeling of the column experiment

4.6.1 Bohart–Admas [9] model

The following expression describes the Bohart–Admas model equation which is the plot of $\ln(C_t/C_0)$ versus t.

$$\ln\left(\frac{C_t}{C_0}\right) = K_{AB}C_0 t - K_{AB}N_0\frac{Z}{u_0} \tag{3}$$

Figures S1 and S2 represent the model plot for Pb(II) ion and Cr(VI) ion removal, respectively. Table 4 represents the Bohart–Admas model parameters K_{AB}, N_o along with correlation coefficient R^2 for Pb(II) ion as well as the Cr(VI) ions removal, respectively. The surface reaction theory is the basic concept of this model which explains the relation between the relative concentration and contact time for the continuous system [31]. The initial portion of the breakthrough curve has been described using this model [31, 45]. From Table 4, it is clear that as bed height increases, N_o is also decreases and as the initial concentration is increased, the N_o is also increased. Similar trends have been found by the researchers [23].

4.6.2 Wolborska model

The Wolborska model is as follow,

$$\ln\left(\frac{C_t}{C_0}\right) = \frac{\beta_a C_0}{q_w}t - \frac{\beta_a Z}{u_0} \tag{4}$$

Wolborska model parameters and correlation coefficient are shown in Table 4 for Pb(II) ion and Cr(VI), respectively [52, 53]. Diffusion in mass transfer is the basic concept of Wolborska model which is applied only for the external diffusion and negligible for axial diffusion. This model is greatly applied to lower metal ion concentration [45]. From Table 4, it is obvious that the increased bed depth

Table 3 Isotherm and kinetics model parameters

Langmuir isotherm model: $\frac{C_e}{q_e} = \frac{1}{a\max} + \frac{c_e}{q\max}$		
Parameters	Value for Pb(II) ion removal	Value for Cr(VI) ion removal
q_{max} (mg g^{-1})	21.38	11.3986
b (L mg^{-1})	0.0455	0.2301
r^2	0.8680	0.9869
Freundlich isotherm model: $\log q_e = \log k_f + \frac{1}{n}\log C_e$		
k_f (mg g^{-1})/(mg L^{-1})$^{1/n}$	1.3248	2.9779
n	1.6560	3.3392
r^2	0.9953	0.9597
Intra-particle diffusion model: $q_t = k_i t^{0.5} + C$ (for removal of Pb(II) ions)		
k_i (mg g^{-1} min$^{1/2}$)	0.0593	
r^2	0.9899	
Pseudo-second-order model: $\frac{dq_t}{dt} = k_2(q_e - q_t)^2$ (for removal of Cr(VI) ions)		
k_2 (mg g^{-1} min^{-1})	0.0132	
r^2	0.9989	

Table 4 Bohart–Admas and Wolborska model parameters for Pb(II) ion and Cr(VI) ion removal

For Pb(II) ion removal

Variation of bed depth

Influent concentration: 10 mg L^{-1}; Flow rate: 10 mL min^{-1}

Bed depth	Bohart–Admas model		Wolborska model		Correlation coefficient R^2
	Rate constant	Saturation concentration	Rate constant	Metal uptake capacity	
Z (cm)	$K_{AB} \times 10^3$ (L mg^{-1})	N_0 (g L^{-1})	β_a (min^{-1})	q_w (g L^{-1} min^{-1})	
4	0.882	35.49	31.34	35.49	0.9820
6	0.764	28.99	22.15	28.99	0.9848
10	0.602	23.92	14.40	23.92	0.9421

Variation of Flow rate

Influent concentration: 20 mg L^{-1}; Bed depth: 10 cm

Flow rate	Bohart–Admas model		Wolborska model		Correlation coefficient R^2
	Rate constant	Saturation concentration	Rate constant	Metal uptake capacity	
v (mL min^{-1})	$K_{AB} \times 10^3$ (L mg^{-1})	N_0 (g L^{-1})	β_a (min^{-1})	q_w (g L^{-1} min^{-1})	
10	0.393	37.59	14.77	37.59	0.9954
30	0.436	31.24	13.62	31.24	0.9683
40	0.428	25.85	11.06	25.85	0.9559

Variation of Influent concentration

Bed depth: 4 cm; Flow rate: 10 mL min^{-1}

Influent concentration	Bohart–Admas model		Wolborska model		Correlation coefficient R^2
	Rate constant	Saturation concentration	Rate constant	Metal uptake capacity	
C_0 (mg L^{-1})	$K_{AB} \times 10^3$ (L mg^{-1})	N_0 (g L^{-1})	β_a (min^{-1})	q_w (g L^{-1} min^{-1})	
10	0.882	35.49	31.34	35.49	0.9820
20	0.5	58.56	29.28	58.56	0.9512
30	0.45	68.97	31.04	68.97	0.8602

For Cr(VI) ion removal

Variation of bed depth

Influent concentration: 10 mg L^{-1}; Flow rate: 10 mL min^{-1}

Bed depth	Bohart–Admas model		Wolborska model		Correlation coefficient R^2
	Rate constant	Saturation concentration	Rate constant	Metal uptake capacity	
Z (cm)	$K_{AB} \times 10^3$ (L mg^{-1})	N_0 (g L^{-1})	β_a (min^{-1})	q_w (g L^{-1} min^{-1})	
4	2.164	12.299	26.62	12.299	0.9433
6	1.683	11.97	20.15	11.97	0.9167
10	3.129	4.37	13.67	4.37	0.7956

Table 4 (continued)

Variation of Flow rate

Influent concentration: 20 mg L^{-1}; Bed depth: 10 cm

Flow rate	Bohart–Admas model		Wolborska model		Correlation coefficient R^2
	Rate constant	Saturation concentration	Rate constant	Metal uptake capacity	
v (mL min^{-1})	$K_{AB} \times 10^3$ (L mg^{-1})	N_0 (g L^{-1})	β_a (min^{-1})	q_w (g L^{-1} min^{-1})	
10	1.494	9.76	14.59	9.76	0.8369
30	2.235	6.66	14.88	6.66	0.9086
40	1.96	6.85	13.42	6.83	0.8420

Variation of Influent concentration

Bed depth: 4 cm; Flow rate: 10 mL min^{-1}

Influent concentration	Bohart–Admas model		Wolborska model		Correlation coefficient R^2
	Rate constant	Saturation concentration	Rate constant	Metal uptake capacity	
C_0 (mg L^{-1})	$K_{AB} \times 10^3$ (L mg^{-1})	N_0 (g L^{-1})	β_a (min^{-1})	q_w (g L^{-1} min^{-1})	
10	2.164	12.299	26.62	12.299	0.9433
20	1.853	19.54	36.21	19.54	0.9672
30	0.791	40.87	32.33	40.87	0.8260

and decreased influent concentration resulted in the decreased metal uptake capacity.

4.6.3 Thomas [46] model

The Thomas model for fixed-bed column adsorption process is presented here in the form of the following equation,

$$\frac{C_t}{C_0} = \frac{1}{1 + \exp\left[k_{th}\left(q_0 x - C_0 V_{eff}\right)v\right]} \tag{5}$$

or,

$$\ln\left(\frac{C_0}{C_t} - 1\right) = \frac{k_{th} q_0 x}{v} - k_{th} C_0 t \tag{6}$$

The model parameters k_{th} and q_o are determined by plotting $\ln\left[\left(\frac{C_o}{C_t}\right) - 1\right]$ versus t. Table 5 presents the model parameters along with the correlation coefficient for Pb(II) ion and Cr(VI) ion, respectively. Figures S3 and S4 present the model plot for Pb(II) ion and Cr(VI) ion adsorption. This model is established by assuming the base of Langmuir isotherm of sorption theory [31]. This model is assumed no axial dispersion, but the external and internal diffusion

take place [28]. Thomas model is applicable for the part of relative concentration less than 0.3 and controlled by the interphase mass transfer concept. Table 5 is explained that the k_{th} is decreased with the increased bed depth and initial concentration and also with the reduced rate of flow.

4.6.4 Yoon–Nelson [54] model

The well-known linearized equation for Yoon–Nelson model is presented as follows,

$$\frac{C_t}{C_0 - C_t} = \exp\left(k_{YN} t - k_{YN} \tau\right) \tag{7}$$

or,

$$\ln\left(\frac{C_t}{C_0 - C_t}\right) = k_{YN} t - \tau k_{YN} \tag{8}$$

The model rate constant as well as the time required for 50% breakthrough has been determined by observing the slope along with the intercept of the plot of $\ln\left[\frac{C_t}{(C_o - C_t)}\right]$ versus t. The capacity of the metal uptake has been determined by the use of the following equation which is the function of influent concentration as well as flow rate and weight of the adsorbent.

Table 5 Thomas and Yoon–Nelson model parameters for Pb(II) ion and Cr(VI) ion removal

For Pb(II) ion removal

Variation of bed depth

Influent concentration: 10 mg L^{-1}; Flow rate: 10 mL min^{-1}

Bed depth	Equilibrium metal uptake	Thomas model			Yoon–Nelson model			
		Rate constant	Maximum metal uptake	Correlation coefficient	Model constant	Time	Metal uptake capacity	Correlation coefficient
Z (cm)	q_{eq} (mg g^{-1})	$k_{th} \times 10^3$ (L mg^{-1} min^{-1})	q_0 (mg g^{-1})	R^2	$k_{yn} \times 10^2$ (min^{-1})	τ (min)	q_y (mg g^{-1})	R^2
4	5.72	1.335	7.8	0.9870	2.03	139.70	5.59	0.9784
6	7.42	0.957	9.92	0.9586	1.59	193.68	6.62	0.9690
10	6.87	0.818	8.41	0.9019	1.36	267.43	6.62	0.8998

Variation of Flow rate

Influent concentration: 20 mg L^{-1}; Bed depth: 10 cm

Flow rate	Equilibrium metal uptake	Thomas model			Yoon–Nelson model			
		Rate constant	Maximum metal uptake	Correlation coefficient	Model constant	Time	Metal uptake capacity	Correlation coefficient
v (mL min^{-1})	q_{eq} (mg g^{-1})	$k_{th} \times 10^3$ (L mg^{-1} min^{-1})	q_0 (mg g^{-1})	R^2	$k_{yn} \times 10^2$ (min^{-1})	τ (min)	q_y (mg g^{-1})	R^2
10	13.86	0.43	15.72	0.9860	0.89	328.81	15.29	0.9856
30	35.30	0.61	32.62	0.9828	1.36	214.66	29.95	0.9884
40	39.16	0.82	27.49	0.9708	1.47	159.64	29.70	0.9937

Variation of Influent concentration

Bed depth: 4 cm; Flow rate: 10 mL min^{-1}

Influent concentration	Equilibrium metal uptake	Thomas model			Yoon–Nelson model			
		Rate constant	Maximum metal uptake	Correlation coefficient	Model constant	Time	Metal uptake capacity	Correlation coefficient
C_0 (mg L^{-1})	q_{eq} (mg g^{-1})	$k_{th} \times 10^3$ (L mg^{-1} min^{-1})	q_0 (mg g^{-1})	R^2	$k_{yn} \times 10^2$ (min^{-1})	τ (min)	q_y (mg g^{-1})	R^2
10	5.72	1.335	7.8	0.9870	2.03	139.70	5.59	0.9784
20	16.10	1.09	9.84	0.9991	1.92	135.20	10.81	0.9890
30	22.99	0.89	9.17	0.9769	2.73	106.32	12.76	0.9383

For Cr(VI) ion removal

Variation of bed depth

Influent concentration: 10 mg L^{-1}; Flow rate: 10 mL min^{-1}

Bed depth	Equilibrium metal uptake	Thomas model			Yoon–Nelson model			
		Rate constant	Maximum metal uptake	Correlation coefficient	Model constant	Time	Metal uptake capacity	Correlation coefficient
Z (cm)	q_{eq} (mg g^{-1})	$k_{th} \times 10^3$ (L mg^{-1} min^{-1})	q_0 (mg g^{-1})	R^2	$k_{yn} \times 10^2$ (min^{-1})	τ (min)	q_y (mg g^{-1})	R^2
4	2.798	3.45	3.34	0.9841	2.57	100.98	4.04	0.9687
6	3.93	1.54	6.78	0.9707	1.48	195.14	6.97	0.9757

Table 5 (continued)

For Cr(VI) ion removal

Variation of bed depth

Influent concentration: 10 mg L^{-1}; Flow rate: 10 mL min^{-1}

Bed depth	Equilibrium metal uptake	Thomas model			Yoon–Nelson model			
		Rate constant	Maximum metal uptake	Correlation coefficient	Model constant	Time	Metal uptake capacity	Correlation coefficient
Z (cm)	q_{eq} (mg g^{-1})	$k_{th} \times 10^3$ (L mg^{-1} min^{-1})	q_0 (mg g^{-1})	R^2	$k_{yn} \times 10^2$ (min^{-1})	τ (min)	q_y (mg g^{-1})	R^2
10	3.25	1.34	5.44	0.9143	1.30	239.45	5.57	0.9299

Variation of Flow rate

Influent concentration: 20 mg L^{-1}; Bed depth: 10 cm

Flow rate	Equilibrium metal uptake	Thomas model			Yoon–Nelson model			
		Rate constant	Maximum metal uptake	Correlation coefficient	Model constant	Time	Metal uptake capacity	Correlation coefficient
v (mL min^{-1})	q_{eq} (mg g^{-1})	$k_{th} \times 10^3$ (L mg^{-1} min^{-1})	q_0 (mg g^{-1})	R^2	$k_{yn} \times 10^2$ (min^{-1})	τ (min)	q_y (mg g^{-1})	R^2
10	7.96	1.64	4.70	0.9325	2.01	141.07	6.56	0.9085
30	18.297	2.13	11.04	0.9373	2.21	122.02	17.02	0.8683
40	11.74	2.30	10.22	0.9847	2.53	78.33	14.57	0.9402

Variation of Influent concentration

Bed depth: 4 cm; Flow rate: 10 mL min^{-1}

Influent concentration	Equilibrium metal uptake	Thomas model			Yoon–Nelson model			
		Rate constant	Maximum metal uptake	Correlation coefficient	Model constant	Time	Metal uptake capacity	Correlation coefficient
C_0 (mg L^{-1})	q_{eq} (mg g^{-1})	$k_{th} \times 10^3$ (L mg^{-1} min^{-1})	q_0 (mg g^{-1})	R^2	$k_{yn} \times 10^2$ (min^{-1})	τ (min)	q_y (mg g^{-1})	R^2
10	2.798	3.45	3.34	0.9841	2.57	100.98	4.04	0.9687
20	8.71	3.20	4.05	0.8550	3.10	75.20	6.01	0.7957
30	10.18	1.82	7.46	0.9646	3.72	79.15	9.50	0.8787

$$q_y = \frac{C_0 \cdot \tau \cdot v}{x} \qquad (9)$$

Table 5 represents the model parameters for Pb(II), and Cr(VI) ion and Figs. S5 and S6 represent the model plot. This model is set up with the assumption that the basics of the probability of the decreased rate in the adsorption for the metal ions are proportional to that of the probability related to the breakthrough of metal ions on adsorbents [24, 28]. The data collected from the experiment fits perfectly with the Yoon–Nelson model which gives the value of the correlation factor very much close to 1.

4.7 Way to dispose of the metal-loaded adsorbent to the environment

The metal-loaded RH disposal is not recommended in the open atmosphere as it may leach. Hence, incineration has been performed with the metal-loaded RH at 680–700 °C temperature to get the ash and then 5 mg of this is mixed with 25 mL of deionized water to get a ratio of liquid–solid in 5:1 [37, 40]. After continuous stirring for 24 h, the metal ions concentration has been analyzed using filtrate. It has been noticed that Pb(II) ion or Cr(VI) are not present in the leach out the solution. Therefore, it can be used as road filling materials.

5 Modeling of the network

The modeling has been performed with a genetic algorithm. The pruning is performed by the use of a very popular ANN training algorithm (Levenberg–Marquardt). The algorithm is applied using a hidden and an output layer for its optimized performance. The data related to Cr(VI) and Pb(II) have been analyzed separately. Researchers [4–7, 11, 16–18, 34, 43, 44] have demonstrated successful predictability using ANN even without normalization. Hence, this analysis is based on the original data. Table 6 helps us to describe the data. The inputs are as follows,

(i)   Bed height (Z)
(ii)   Effluent concentration (C_t)
(iii) Flow rate (v)
(iv)   Inlet concentration (C_o)
(v)   Time (t)

The data related to pH are constant, so it has not been part of the analysis for both the metals. Percentage removal is considered to be the output variable. The data sets are randomized (for three times separately) for the removal of the possibility of random error. All of the three data sets have been analyzed (three times) independently. From the overall data, 70% and 20% have been used for training and cross-validation, respectively. Then, the rest of the 10% have been used for prediction purpose.

Genetic algorithm (GA) is applied for pruning the network and its optimized output. GA is used to consider only the optimized inputs. GA also optimizes the number of hidden layers processing elements. The process of GA also requires the choice of selection, crossover and mutation rules. For this analysis, 'roulette selection rule' has been considered. The crossover probability applicable to one point crossover rule is applied with a value of 0.9, and the probability applicable to mutation using uniform mutation rule is applied with a value of 0.1. The variability related to the processing element number is kept between 1 and 25. The values related to the population sizes are 60 and 70 for Cr(VI) and Pb(II), respectively. A maximum generation number used for the evolution is 100 for both the networks.

The use of the Levenberg–Marquardt algorithm has been described mainly by the following three points,

(i)   The hyperbolic tangent transfer function has been applied within the hidden and the output layer.
(ii)   The 10^3 epochs have been set for each run.
(iii) The LM algorithm is programmed to stop within the maximum of 10^2 consecutive epochs if the value of MSE associated with cross-validation is not observed.

### 5.1 Performance of the network

The value of the cross-correlation coefficient is an obvious choice for the performance of the GA output. However, AARE is also one of the performance indicators for network output along with the values of MSE as well as SD. The smaller the values of these statistical parameters, the better are the performance of the network. By observing

Table 6 Range of experimental and GA analysis data

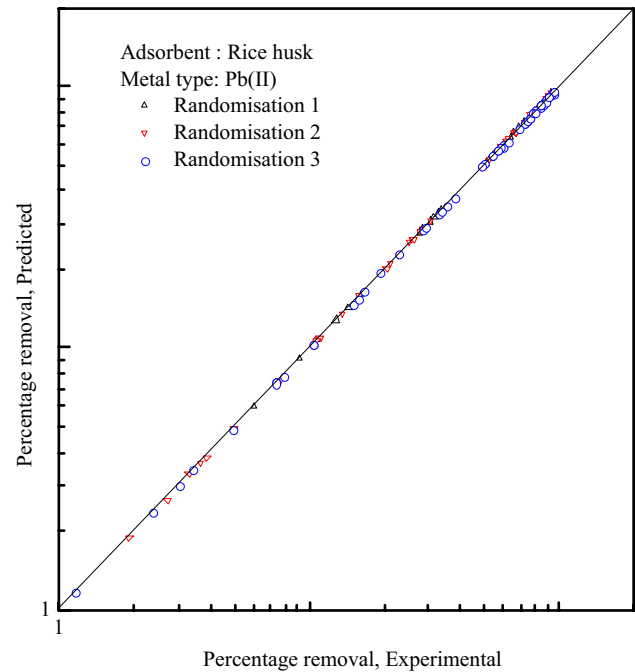| Metal type	Measurement type		Range
Name of adsorbent: rice husk			
Cr(VI)	Input parameters	pH	2
		Bed height, Z (cm)	4–10
		Flow rate, v (mL/min)	10–40
		Contact time, t (min)	10–460
		Initial concentration, C_o (mg/L)	10.00–30.00
		Effluent concentration, C_t (mg/L)	0.136–29.92
	Output parameter	Percentage removal (%)	0.26667–98.64
	Total number of data points		431
Pb(II)	Input parameters	pH	5
		Bed height, Z (cm)	4–10
		Flow rate, v (mL/min)	10–40
		Contact time, t (min)	10–620
		Initial concentration, C_o (mg/L)	10.00–30.00
		Effluent concentration, C_t (mg/L)	0.32–29.93
	Output parameter	Percentage removal (%)	0.23333–96.80
	Total number of data points		565

Table 7 Performance of the optimized hybrid network for three different randomization for the prediction of percentage removal

Metal type	Randomiza-tion No.	Minimum MSE of cross-validation	AARE	SD (σ)	MSE	CCC (R)
Cr(VI)	1	3.06×10^{-8}	0.003398	0.008469	0.000167	1
	2	2.19×10^{-7}	0.010673	0.042232	0.000356	1
	3	2.57×10^{-8}	0.011857	0.039236	0.000415	1
Pb(II)	1	1.05×10^{-8}	0.000859	0.002785	4.20×10^{-5}	1
	2	2.46×10^{-8}	0.001242	0.004114	1.93×10^{-4}	1
	3	2.63×10^{-8}	0.001389	0.003896	6.78×10^{-5}	1
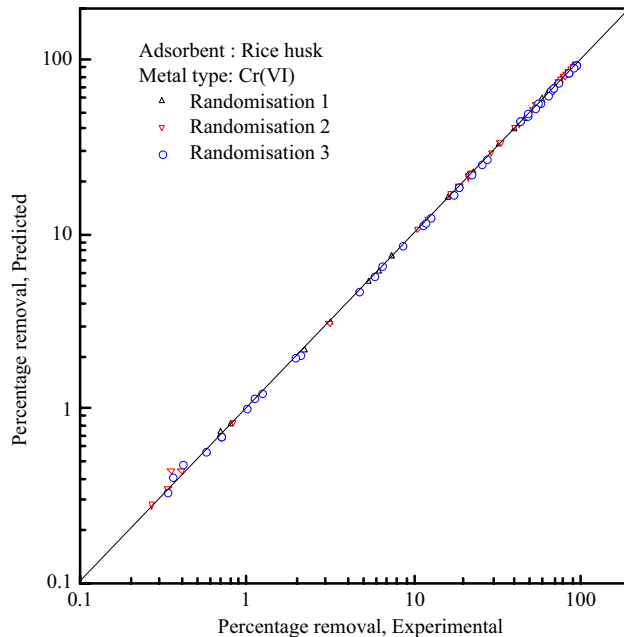
Fig. 9 Comparison of percentage removal for experimental to the GA–ANN prediction for Cr(VI)

Fig. 10 Comparison of percentage removal for experimental to the GA–ANN prediction for Pb(II)

this value, the proper statistical validity of the input and the output can be found out. Figures S7 and S8 show the change in the value of minimum cross-validation MSE resulted out of every generation with that of the generation number for the different randomization number. The optimized condition of the proposed network is considered when the minimum cross-validation MSE is achieved for one particular generation. From Table 7, the minimum value of MSE for the pruning process as well as the final error values for both analyses can be observed.

Table 7 represents the final prediction value of the GA–NN networks. It can be observed that the value of R related to the final prediction is unity in the case of the removal of both the metals. The extremely low value of all the statistical error parameters, i.e., MSE, SD, and AARE indicate the accurate result concerning the final prediction. From both the results, it is clear that GA–NN model can predict the percentage removal successfully. Figures 9

and 10 show the comparison of the values acquired from the experiment to the GA–NN prediction for all different randomizations as mentioned above. The results (Table 7) and the observations of Figs. 9 and 10 are proof of good performance.

Finally, it can be said that the use of the neural network with genetic algorithm produces an excellent result for the prediction of percentage removal of heavy metals.

6 Conclusions

The column study established the suitability of rice husk for Pb(II) as well as Cr(VI) ions. The packed-bed continuous column experiment is the function of contact time, flow rate, bed height. The operating parameters are varied to evaluate the breakthrough curve for the column

performance. The breakthrough, as well as the exhaustion time, can be increased by increasing the bed depth but these parameters decrease when both influent concentrations, as well as the flow rate, are increased. The data are well fitted to these models and give a good prediction to the theoretical value. From the statistical analysis, it is obtained that Thomas model, as well as the Yoon–Nelson model, agree well with the column performance of rice husk as these models give the value of R^2 0.9019–0.9991 for Pb(II) removal, 0.8550–0.9847 for Cr(VI) removal and 0.8998–0.9937 for Pb(II) removal, 0.7957–0.9687 for Cr(VI) removal, respectively.

A network using Genetic algorithm pruned with Levenberg–Marquardt algorithm has been used for the analysis. The observation of the results indicates that this GA–NN modeling has predicted the % removal of Pb(II) ion and Cr(VI) ion well.

A low cost, practically little-used material is tried as an adsorbent. Adsorptive capacity realized is moderate and not as high as reported with other synthetic adsorbents. These demand the use of a higher amount of adsorbent and a bigger size of the equipment. This is offset by the advantages of very low cost of the adsorbent and associated reduction in the costs involved in the recovery of adsorbent and ease of disposal.

Compliance with ethical standards

Conflict of interest The authors declare that they have no conflict of interest.

References

1. Aguayo-Villarreal IA, Bonilla-Petriciolet A, Hernandez-Montoya V, Montes-Moran MA, Reynel-Avila HE (2011) Batch and column studies of Zn^{2+} removal from aqueous solution using chicken feathers as sorbents. J Chem Eng 167:67–76
2. APHA, AWWA, WEF (1998) Standard methods for the examination of water and wastewater, 20th edn. American Public Health Association, American Water Works Association and Water Environmental Federation, Washington, DC
3. Avila M, Burks T, Akhtar F, Götheli G, Lansåker PC, Toprak MS, Muhammed M (2014) Surface functionalized nanofibers for the removal of chromium(VI) from aqueous solutions. J Chem Eng 245:201–209
4. Banerjee M, Bar N, Basu RK, Das SK (2018) Removal of Cr(VI) from its aqueous solution using green adsorbent pistachio shell: a fixed bed column study and GA–ANN modelling. Water Conser Sci Eng 3:19–31
5. Bar N, Bandyopadhyay TK, Biswas MN, Das SK (2010) Prediction of pressure drop using artificial neural network for non-Newtonian liquid flow through piping components. J Pet Sci Eng 71:187–194
6. Bar N, Biswas MN, Das SK (2010) Prediction of pressure drop using artificial neural network for gas-non-Newtonian liquid flow through piping components. Ind Eng Chem Res 49:9423–9429
7. Bar N, Das SK (2011) Comparative study of friction factor by prediction of frictional pressure drop per unit length using empirical correlation and ANN for gas-non-Newtonian liquid flow through 180° circular bend. Int Rev Chem Eng 3(6):628–643
8. Bhattacharya AK, Naiya TK, Mandal SN, Das SK (2008) Adsorption, kinetics and equilibrium studies on removal of Cr(VI) from aqueous solution using different low-cost adsorbents. J Chem Eng 137:529–541
9. Bohart G, Admas EN (1920) Some aspects of the behavior of charcoal with respect to chlorine. J Am Chem Soc 42:523–544
10. Chen S, Yue Q, Gao B, Li Q, Xu X, Fu K (2012) Adsorption of hexavalent chromium from aqueous solution by modified cornstalk: a fixed-bed column study. Bioresour Technol 113:114–120
11. Das B, Ganguly UP, Bar N, Das SK (2015) Holdup prediction in inverse fluidization using non-Newtonian pseudoplastic liquids: empirical correlation and ANN modeling. Powder Technol 273:83–90
12. Demirbas A (2008) Heavy metal adsorption onto agro-based waste material: a review. J Hazard Mater 157(2–3):220–229
13. EPA: United State Environmental Protection Agency (1990) Cincinnati OH USA
14. Feng Q, Lin Q, Gong F, Sugita S, Shoya M (2004) Adsorption of lead and mercury by rice husk ash. J Colloid Interface Sci 278:1–8
15. Foo KY, Hameed BH (2009) Utilization of rice husk ash as novel adsorbent: a judicious recycling of the colloidal agricultural waste. Adv Colloid Interface Sci 152:39–47
16. Ghaedi M, Ghaedi AM, Adbi F, Roosta M, Sahraei R, Daneshfar A (2014) Principal component analysis-artificial neural network and genetic algorithm optimization for removal of reactive orange 12 by copper and nanoparticles-activated carbon. J Ind Eng Chem 20:787–795
17. Ghaedi M, Daneshfar A, Ahmadi A, Momeni MS (2015) Artificial neural network-genetic algorithm based optimization for the adsorption of phenol red (PR) onto gold and titanium dioxide nanoparticles loaded on activated carbon. J Ind Eng Chem 21:587–598
18. Ghaedi AM, Ghaedi M, Pouranfard AR, Ansari A, Avazzadeh Z, Vafaei A, Agarwal S, Gupta VK, Tyagie I (2016) Adsorption of Triamterene on multi-walled and single-walled carbon nanotubes: artificial neural network modeling and genetic algorithm optimization. J Mol Liq 216:654–665
19. Goel J, Kadirvelu K, Rajagopal C, Garg VK (2005) Removal of lead(II) by adsorption using treated granular activated carbon: batch and column studies. J Hazard Mater B125:211–220
20. Han R, Ding D, Xu Y, Zou W, Wang Y, Li Y, Zou L (2008) Use of rice husk for the adsorption of congo red from aqueous solution in column mode. Bioresour Technol 99(8):2938–2946
21. IS 10500:1991 (1991) Bureau of Indian standards. Drinking Water Specifications, New Delhi
22. Jain M, Garg VK, Kadirvelu K (2013) Cadmium(II) sorption and desorption in a fixed bed column using sunflower waste carbon calcium-alginate beads. Bioresour Technol 129:242–248
23. Karimi M, Shojaei A, Nematollahzadeh A, Abdekhodaie MJ (2012) Column study of Cr (VI) adsorption onto modified silica–polyacrylamide microspheres composite. Chem Eng J 210:280–288

24. Khalir WKAWM, Hanafiah MAKM, So'ad SZM, Ngah WSW, Majid ZAZ (2012) Batch, column and thermodynamic of Pb(II) adsorption on xanthated rubber (*Hevea brasiliensis*) leaf powder. J Appl Sci 12(11):1142–1147

25. Kumar S, Mohanta K, Kumar D, Prakash O (2012) Properties and industrial applications of rice husk: a review. Int J Emerg Technol Adv Eng 2(10):86–90

26. Kumar S, Sangwan P, Dhankhar R, Mor V, Bidra S (2013) Utilization of rice husk and their ash: a review. Res J Chem Environ Sci 1(5):126–129

27. Kyzas Z, Kostoglou M (2014) Green adsorbents for wastewaters: a critical review. Materials 7:333–364

28. Lalhruaitluanga H, Jayaram K, Prasad MNV, Kumar KK (2010) Lead(II) adsorption from aqueous solutions by raw and activated charcoals of *Melocanna baccifera* Roxburgh (bamboo)—a comparative study. J Hazard Mater 175:311–318

29. Li K, Wang X (2009) Adsorptive removal of Pb(II) by activated carbon prepared from *Spartina alterniflora*: equilibrium, kinetics and thermodynamics. Bioresour Technol 100:2810–2815

30. Li W, Zhang L, Peng Z, Li N, Zhang S, Guo S (2008) Tobacco stems as a low cost adsorbent for the removal of Pb(II) from wastewater: equilibrium and kinetic studies. Ind Crops Prod 28:294–302

31. Long Y, Lei D, Ni J, Ren Z, Chen C, Xu H (2014) Packed bed column studies on lead(II) removal from industrial wastewater by modified *Agaricus bisporus*. Bioresour Technol 152:457–463

32. Luduena L, Fasce D, Alvarez VA, Stefani PM (2011) Nanocellulose from rice husk following alkaline treatment to remove silica. BioResources 6(2):1440–1453

33. Mitra T, Das SK (2016) Adsorptive removal of Cr(VI) from aqueous solution using blackberry leaves-column study. Int J Environ Eng 8(4):225–244

34. Mitra T, Singha B, Bar N, Das SK (2014) Removal of Pb(II) ions from aqueous solution using water hyacinth root by fixed-bed column and ANN modelling. J Hazard Mater 273:94–103

35. Mobasherpour I, Salahi E, Asjodi A (2014) Research on the batch and fixed-bed column performance of red mud adsorbents for lead removal. Can Chem Trans 2(1):83–96

36. Mondal MK (2009) Removal of Pb(II) ions from aqueous solution using activated tea waste: adsorption on a fixed-bed column. J Environ Manag 90:3266–3271

37. Nag S, Mondal A, Mishra U, Bar N, Das SK (2016) Removal of chromium(VI) from aqueous solutions using rubber leaf powder: batch and column studies. Desalin Water Treat 57(36):16927–16942

38. Nguyen TAH, Ngo HH, Guo WS, Zhang J, Liang S, Yue QY, Li Q, Nguyen TV (2013) Applicability of agricultural waste and by-products for adsorptive removal of heavy metals from wastewater. Bioresour Technol 148:574–585

39. Saçmaci Ş, Kartal Ş, Yılmaz Y, Saçmaci M, Soykan C (2012) A new chelating resin: synthesis, characterization and application for speciation of chromium (III)/(VI) species. Chem Eng J 181–182:746–753

40. Sarode DB, Jadhav RN, Khatik VA, Ingle ST, Attrade SB (2010) Extraction and leaching of heavy metals from thermal power plant fly ash and Its admixtures. Pol J Environ Stud 19(6):1325–1330

41. Singha B, Das SK (2011) Biosorption of Cr(VI) ions from aqueous solutions: kinetics, equilibrium, thermodynamics and desorption studies. Colloids Surf B Biointerfaces 84:221–231

42. Singha B, Das SK (2012) Removal of Pb(II) ions from aqueous solution and industrial effluent using natural biosorbents. Environ Sci Poll Res 19:2212–2226

43. Singha B, Bar N, Das SK (2014) The use of artificial neural networks (ANN) for modeling of adsorption of Cr(VI) ions. Desalin Water Treat 52(1–3):415–525

44. Singha B, Bar N, Das SK (2015) The use of artificial neural network (ANN) for modeling of Pb(II) adsorption in batch process. J Mol Liq 211:228–232

45. Sugashini S, Begum KMMS (2013) Performance of ozone treated rice husk carbon (OTRHC) for continuous adsorption of Cr(VI) ions from synthetic effluent. J Environ Chem Eng 1:79–85

46. Thomas HG (1948) Chromatography: a problem in kinetics. Ann N Y Acad Sci 49(2):161–182

47. Tong S, Schirnding Y, Von E, Prapamontol T (2000) Environmental lead exposure: a public health problem of global dimensions. Bull World Health Organ 78(9):1068–1077

48. Uluozlu OD, Sari A, Tuzen M, Soylak M (2008) Biosorption of Pb(II) and Cr(III) from aqueous solution by lichen (*Parmelina tiliacea*) biomass. Bioresour Technol 99:2972–2980

49. Unuabonah EI, Olu-Owolabi BI, Adebowale KO, Ofomaja AE (2007) Adsorption of lead and cadmium ions from aqueous solutions by tripolyphosphate-impregnated Kaolinite clay. Colloids Surf A Physicochem Eng Asp 292:202–211

50. Vinodhini V, Das N (2010) Packed-bed column studies on Cr(VI) removal from tannery wastewater by neem sawdust. Desalination 264:9–14

51. WHO: World Health Organization (1993) Guidelines for drinking water quality, vol 1. Geneva, p 52

52. Wolborska A (1989) Adsorption on activated carbon of p-nitrophenol from aqueous solution. Water Res 23:85–91

53. Wolborska A, Pustelnik P (1996) A simplified method for determination of break-through time of an adsorbent layer. Water Res 30:2643–2650

54. Yoon YH, Nelson JH (1984) Application of gas adsorption kinetics II A theoretical model for respirator cartridge service life. Am Ind Hygiene Ass J 45:509–516

Web site

55. https://www.mordorintelligence.com/industry-reports/global-activated-carbon-market, seen on dated 13.06.2017